IJST, Transactions of Civil Engineering, Vol. 37, No. C1, pp 111-126
Printed in The Islamic Republic of Iran, 2013

CORRELATION BETWEEN SETTLEMENT OF EMBANKMENT DAMS AND GROUND MOTION INTENSITY INDICES OF PULSE-LIKE RECORDS*

N. HADIANI[1],** M. DAVOODI[2] AND M.K. JAFARI[3]

[1]Dept. of Civil Engineering, Science and Research Branch, Islamic Azad University, Tehran, I. R. of Iran
Email: n.hadiani@gmail.com
[2,3]Dept. of Geotechnical Earthquake Engineering, International Institute of Earthquake Engineering and Seismology, Tehran, I. R. of Iran

Abstract– Near-fault seismic records strongly influenced by forward directivity are characterized by one or more large pulses in velocity time histories. The characteristics of these records are significantly different from ordinary records. This study evaluated the correlation between the intensity indices of pulse-like ground motion and crest settlement of embankment dams and their ranking according to quality was evaluated. The seismic behavior of five embankment dams with different heights was investigated under 105 pulse-like and 20 ordinary ground motions with over 680 nonlinear time history analyses. The results showed that inelastic structural ground motion intensity indices are more applicable than elastic indices to predict the settlement of embankment dams. The proposed inelastic structural ground motion intensity (I_{MPD}) calculates the mean permanent displacement of a single degree of freedom (SDOF) system over a period of $0.2T_1$ to $1.5T_1$ (where T_1 is the natural period of the dam) based on Newmark's method using a decoupled approximation and deformable SDOF instead of a rigid block system. The non-structure ground motion intensity index I_{VA} (where I_{VA} is the square root of the product of peak ground velocity and plain integral of the squared acceleration) is proposed as a good predictor for the nonlinear response of embankment dams.

Keywords– Pulse-like, ground motion intensity index, embankment dam

1. INTRODUCTION

Near-fault ground motion is typically assumed to be restricted to within 20 to 30 km of a fault. However, this definition is not universal because near-fault effects attenuate as distance increases which, in turn, leads to a greater effect of factors such as magnitude and local site conditions on ground motion. The distinguishing characteristics of near-fault ground motion are the pulses generated by the directivity and fling-step effects. These pulse-like ground motions often contain one or more distinct pulses in the acceleration, velocity and displacement time histories, most frequently in velocity [1].

A challenging issue in seismic risk analyses and performance-based earthquake engineering is the determination of the correlation between damage suffered by structures and ground motion intensity indices. Most studies thus far have been limited to the responses of a single degree of freedom (SDOF) system [2, 3] and building structure response [4-6]. There has been no study in this field on embankment dams.

Research on the relationship between the intensity indices of near-fault ground motion and structural demand parameters is scarce and there are no widely-accepted indices representing the intensity of near-

*Received by the editors November 24, 2011; Accepted October 10, 2012.
**Corresponding author

fault ground motion [7, 8]. Studies on the effect of near-fault ground motion on the seismic behavior of dams and slope stabilities are limited [9, 10] and all agree that the effect of near-fault ground motion is great. Bayraktar [9] used one near-fault and one far-field ground motion to show that near-fault ground motion can create larger displacement and stress in concert dams. Gazetas [10] used simple pulse-like ground motion to represent near-fault ground motion to calculate slope displacement under excitation. He concluded that upper-bound sliding displacement from near-fault excitation may substantially exceed the values obtained from some currently available design charts.

This study evaluated the correlation between the intensity indices of pulse-like ground motion and the seismic response of embankment dams and their ranking according to quality was evaluated. For this purpose, 105 pulse-like near-fault records were used as input ground motions. In addition, 20 ordinary records (without pulse in velocity time history) were used for compression with pulse- like records.
The settlement of embankment dams was selected as the demand response and was calculated using over 680 nonlinear time history analyses for four hypothetical dams with different heights and a real embankment dam.

2. ELASTIC GROUND MOTION INTENSITY INDICES

Generically, the intensity indices of ground motion contain acceleration-related, velocity-related, displacement-related and compound parameters. The first three indices are only appropriate when the systems are high-frequency, intermediate frequency and low frequency, respectively. Furthermore, some intensity indices are dependent on the dynamic characteristics of a structure, such as the pseudo spectral acceleration at the natural period of a structure ($PSa(T_1)$). Others are non-structure-specific (or period-independent), such as peak ground acceleration. The simplest and the most commonly known ground motion intensity indices (GMIIs) are peak ground acceleration (PGA), peak ground velocity (PGV), and peak ground displacement (PGD) and are available from the ground motion record. The plain integral of the squared acceleration (a_{sq}), squared velocity (v_{sq}) and squared displacement (d_{sq}) are used as GMIIs, where t_f is the total duration of the ground motion.

$$a_{sq} = \int_0^{t_f} a^2(t)dt \quad (a), \qquad v_{sq} = \int_0^{t_f} v^2(t)dt \quad (b), \qquad d_{sq} = \int_0^{t_f} d^2(t)dt \quad (c) \tag{1}$$

Other measures of seismic destructiveness can be obtained by the mean-square value of the acceleration history (a_{ms}), the mean-square value of the velocity history (v_{ms}) and the mean-square value of the displacement history (d_{ms}). These GMIIs are:

$$a_{ms} = \frac{1}{t_2 - t_1}\int_{t_1}^{t_2} a^2(t)dt \quad (a), \qquad v_{ms} = \frac{1}{t_2 - t_1}\int_{t_1}^{t_2} v^2(t)dt \quad (b), \qquad d_{ms} = \frac{1}{t_2 - t_1}\int_{t_1}^{t_2} d^2(t)dt \quad (c) \tag{2}$$

In this study, the interval between t_1 and t_2 is the significant duration (t_d) of motion; the interval between instants t_5 and t_{95} ($t_d = t_{95} - t_5$) [11]. Other common intensity parameters that may be calculated from the ground motion trace are the Arias intensity, cumulative absolute velocity and displacement. The Arias index was proposed as a measure of earthquake intensity by calculating the integral of the squared acceleration (Eq. (3)). It is interpreted as the sum of the energies dissipated per unit of mass by a population of damped oscillators of all natural frequencies where g is the acceleration of gravity [12].

$$I_A = \frac{\pi}{2g}\int_0^{t_f} a^2(t)dt \tag{3}$$

GMIIs are based on the time integral of the absolute ground velocity, and displacement are cumulative absolute velocity (CAV) and cumulative absolute displacement (CAD). These GMIIs are calculated as:

$$CAV = \int_0^{t_f} |a(t)|dt \quad (a) \qquad CAD = \int_0^{t_f} |v(t)|dt \quad (b) \tag{4}$$

Fajfar et al. [13] proposed a compound index as a measure of the ground motion capacity to damage structures with fundamental periods in the intermediate period range:

$$I_F = PGV \cdot t_d^{0.25} \tag{5}$$

Riddell and Garcia [14] proposed similar GMIIs that can minimize the dispersion of hysteretic energy dissipation spectra for inelastic systems at three frequency sets. These GMIIs are calculated as:

$$I_a = PGA \cdot t_d^{\frac{1}{3}} \quad (a), \qquad I_v = PGV^{\frac{2}{3}} \cdot t_d^{\frac{1}{3}} \quad (b), \qquad I_d = PGD \cdot t_d^{\frac{1}{3}} \quad (c) \tag{6}$$

PGV/PGA is a compound intensity index that describes the frequency characteristics of ground motion and is also employed to characterize the intensity of near-fault ground motion. If the PGV/PGA ratio is large, it means that the ground motion may have a long-period velocity pulse. The square root of the product of peak ground velocity and plain integral of the squared acceleration (I_{VA}) is proposed as a newly compounded GMII:

$$I_{VA} = \sqrt{PGV \cdot a_{sq}} \tag{7}$$

Correlation coefficients between I_{VA} and other GMIIs are summarized in Table 1.The spectral acceleration at the fundamental period of a structure, PSa, is a widely employed parameter obtained from the pseudo-acceleration response spectrum. Other common structural GMIIs computed from the response spectra of the ground motion record are the Housner intensity (HI) [15], acceleration spectrum intensity (ASI) [16], effective peak acceleration (EPA) and effective peak velocity (EPV) [17].

Table 1. Correlation coefficient between I_{VA} and other GMIIS for pulse-like records

GMII	PGA	I_A	a_{ms}	I_a	PGV	v_{sq}	v_{ms}	IF	I_v	CAV
ρ	65	95	68	80	87	63	79	76	61	76
GMII	PGV/PGA	PGD	d_{sq}	d_{ms}	I_d	CAD	EPA	ASI	EPV	HI
ρ	12	44	32	42	36	48	64	64	80	90

HI is calculated as the area under the pseudo-velocity spectrum (5% damped) of a ground motion for a period of 0.1–2.5 s. This parameter captures important aspects of the amplitude and frequency content (of primary importance for structures) in a single parameter. ASI is defined as the area under the elastic pseudo-acceleration spectrum (5% damped) for a period of 0.1–0.5 s. This parameter is introduced to characterize strong ground motion for the analysis of structures that have fundamental periods of less than 0.5 s. The HI and ASI ground motion intensity indices are calculated as:

$$HI = \int_{0.1}^{2.5} PSV(T, \xi = 0.05)dT \tag{8}$$

$$ASI = \int_{0.1}^{0.5} PSA(T, \xi = 0.05)dT \tag{9}$$

In Eq. (10), the EPA is calculated as the mean pseudo-acceleration spectrum (5% damped) for a period of 0.1-0.5 s divided by the empirical factor 2.5. EPV is the elastic 5%-damped pseudo-velocity spectrum at period T = 1s divided by 2.5:

$$EPA = \left(Mean\left(PSa\left(T_i, i = 0.1,...,05\right)\right)\right)/2.5 \quad \text{for } \xi = 0.05 \tag{10}$$

Current performance-based seismic design and evaluation methodologies prefer the intensity index, which is the mean of the elastic response spectrum for a period of $0.2T_1$ to $1.5T_1$ (where T_1 is the natural period of the structure) [18, 19]. This intensity index, I_{DC}, is calculated as:

$$I_{DC} = Mean\left(PSa\left(T_i, i = 0.2T_1,...,1.5T_1\right)\right) \quad \text{for } \xi = 0.05 \tag{11}$$

3. INELASTIC GROUND MOTIONS INTENSITY INDICES

GMIIs based on elastic response, such as design spectrum intensity (I_{DS}), do not consider the inelastic behavior of a structure and may not be appropriate for near-fault sites where the inelastic deformation can be significantly larger than the deformation of the corresponding linear system. For such sites, scaling methods and GMIIs based on inelastic deformation are more appropriate. In addition to non-structural and elastic structural GMIIs, four inelastic GMIIs have been examined for their correlations with crest settlement in embankment dams. These methods are based on the Newmark displacement method [20] which introduced a simple model to estimate coseismal slope displacement. Newmark' displacement can be used to investigate the effect of ground motion on the nonlinear behavior of geotechnical structures [21] and also to evaluate seismic shear strength of landslides by back-calculation method [22].

Originally, the Newmark method modeled a landslide as a rigid friction block that slides on an inclined plane when subjected to base accelerations approximating an earthquake. Landslide displacement is estimated by integrating twice with respect to time over portions of an earthquake acceleration-time history that exceed the yield acceleration (k_y) required to overcome basal resistance and initiate sliding. It can be calculated based on the geometry of the model and shear strength parameters of the geotechnical structure. Because the Newmark method does not consider the effects of elastic dynamic response, other studies refined and expanded on it to account for the deformability of the system and the dynamic displacement. These approaches generally fall into the categories of coupled and decoupled methods. In coupled methods, the dynamic response and slip displacement are simultaneously taken into account in the solution of the differential equation. In the decoupled methods, the computation of the dynamic response and slip displacement can be decoupled and carried out separately. To measure permanent displacement using the decoupled method, the system can be classified as a SDOF, a series of SDOF, or a generalized mass system [23, 24].

For example, to calculate the permanent displacement of a SDOF system using the decoupled method, the absolute acceleration time history response of the SDOF system on the interested frequency is obtained using Eq. (12). In this equation, ω_n is the undammed natural frequency of the system, ξ is the damping ratio and a_g is the ground acceleration. This absolute acceleration time history is then used in a Newmark method analysis to obtain permanent displacement.

$$\ddot{y} + 2\xi\omega_n\dot{y} + \omega_n^2 y = -a_g(t) \tag{12}$$

The procedure used to obtain Newmark's displacement of record No.17 assuming $k_y = 0.1g$ is shown in Fig. 1a. In addition, the absolute acceleration and permanent displacement spectrums of the SDOF system calculated using the decoupled method are shown in Figs. 1b and 1c for this record.

The inelastic GMIIs used in this study are: ND, Newmark's displacement; PDD (T_1), permanent displacement of the SDOF system (5% damped) using the decoupled method at the natural period of an embankment dam (T_1); I_{MPD}, the mean permanent displacement of SDOF for a period of $0.2T_1$ to $1.5T_1$

calculated using the decoupled method (Eq. (13)); I_{HPD}, the mean permanent displacement of SDOF for a period of 0.1-2.5 s calculated using the decoupled method (Eq. (14)):

$$I_{MPD} = \text{Mean}\left(\text{PDD}\left(T_i, i = 0.2T_1,...,1.5T_1\right)\right) \quad \text{for } \xi = 0.05 \tag{13}$$

$$I_{HPD} = \text{Mean}\left(\text{PDD}\left(T_i, i = 0.1,...,2.5\right)\right) \quad \text{for } \xi = 0.05 \tag{14}$$

Referring to the concept of I_{MPD} and I_{HPD}, they can be used as posterior intensity index for selection and scaling ground motion for use in nonlinear dynamic analyses such as seismic stability of slopes or nonlinear seismic response of embankment dams.

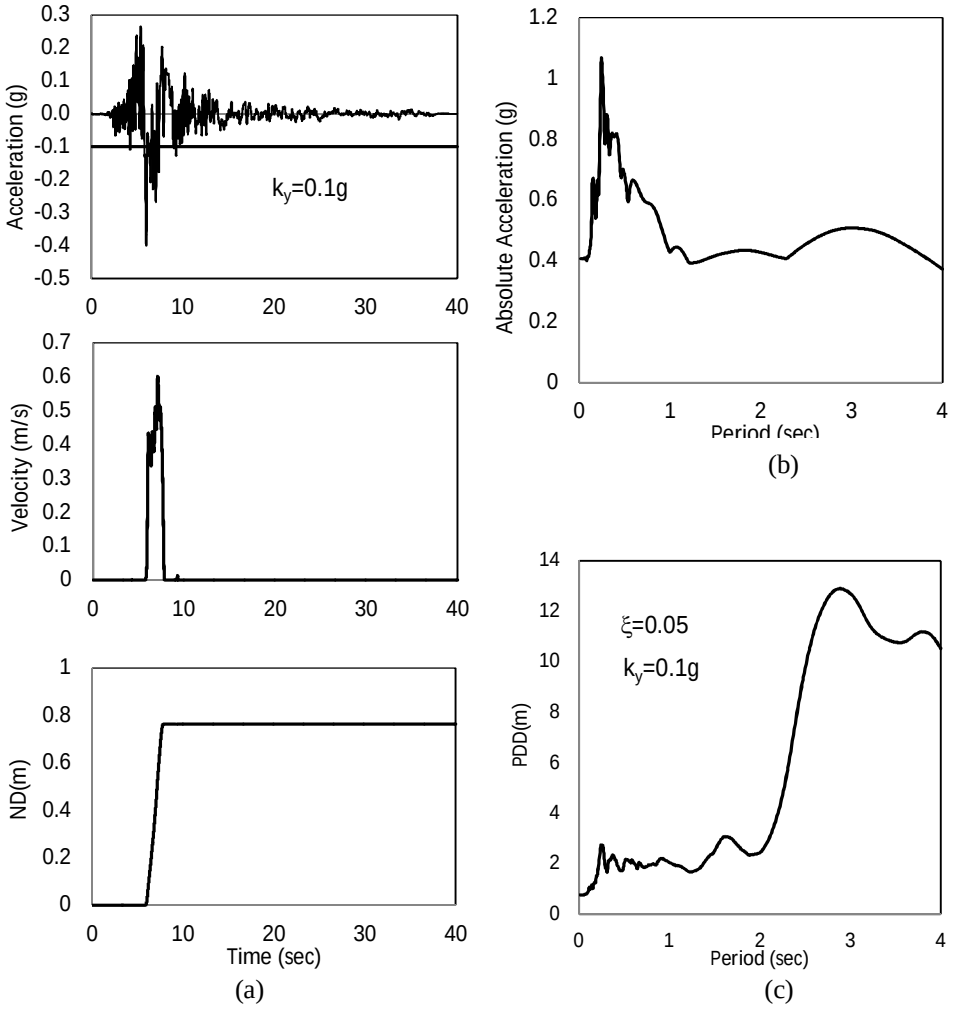

Fig. 1. a) The procedure to obtain Newmark's displacement of record No.17; b) absolute acceleration spectrum of record No.17; c) permanent displacement spectrum of record No.17

4. GROUND MOTION

To investigate the correlation between the seismic response of an embankment dam and different GMIIs, a database of 105 unscaled pulse-like earthquake ground motion records identified as having distinct velocity pulses and 20 unscaled ordinary earthquake ground motion records were selected from the Next Generation Attenuation (NGA) project [25]. Record sequence numbers of the selected ground motions are listed in Table 2. Pulse-like ground motions were oriented in the fault-normal direction. Fig. 2 shows the velocity-time history of pulse-like record No.17 as an example. The ground motion set employed covered

a wide range of earthquake intensities that impose responses in the elastic and inelastic ranges for the embankment dams analyzed. Fig. 3 presents the distribution of the pulse-like ground motion given in Table 2 as a function of earthquake magnitude and closest distance to rupture. The distance range covered suggests that the records represent near-fault ground motions. Near-fault records having distances of less than 30 km dominate the set. The distributions of PGA, PGV and PGD for the selected pulse-like ground motion set are depicted in Fig. 4. As seen, a wide range of ground motions intensities are covered by the ground motions selected.

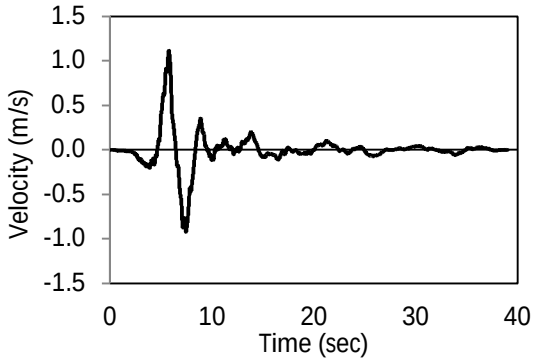

Fig. 2. Velocity time history of record No.17

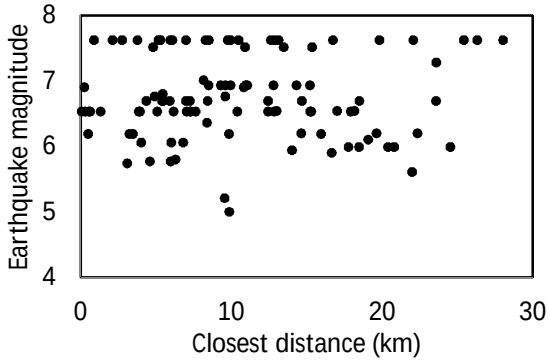

Fig. 3. Magnitude and distance distribution of the ground motion used in the present study

Table 2. Pulse-like and ordinary earthquake ground motion record selected from PEER NGA database

Pulse-like records										Ordinary records	
No	NGA	No	NGA	No	NGA	No	NGA	No	NGA	No	NGA
1	33	23	250	45	719	67	1016	89	1496	1	15
2	126	24	292	46	721	68	1045	90	1499	2	57
3	150	25	316	47	728	69	1050	91	1510	3	326
4	158	26	367	48	752	70	1052	92	1511	4	355
5	159	27	407	49	763	71	1119	93	1515	5	470
6	161	28	415	50	764	72	1148	94	1519	6	520
7	165	29	418	51	765	73	1158	95	1528	7	535
8	167	30	448	52	766	74	1161	96	1530	8	551
9	170	31	451	53	767	75	1176	97	1531	9	621
10	171	32	459	54	768	76	1182	98	1548	10	672
11	173	33	461	55	802	77	1202	99	1550	11	701
12	174	34	495	56	803	78	1244	100	1642	12	761
13	175	35	496	57	821	79	1476	101	1752	13	773
14	178	36	517	58	828	80	1477	102	1853	14	776
15	179	37	529	59	900	81	1480	103	2457	15	900
16	180	38	540	60	959	82	1481	104	2495	16	944
17	181	39	568	61	960	83	1483	105	2627	17	988
18	182	40	595	62	982	84	1484			18	1003
19	183	41	615	63	983	85	1486			19	1039
20	184	42	645	64	1004	86	1489			20	1043
21	185	43	668	65	1009	87	1493				
22	192	44	692	66	1013	88	1494				

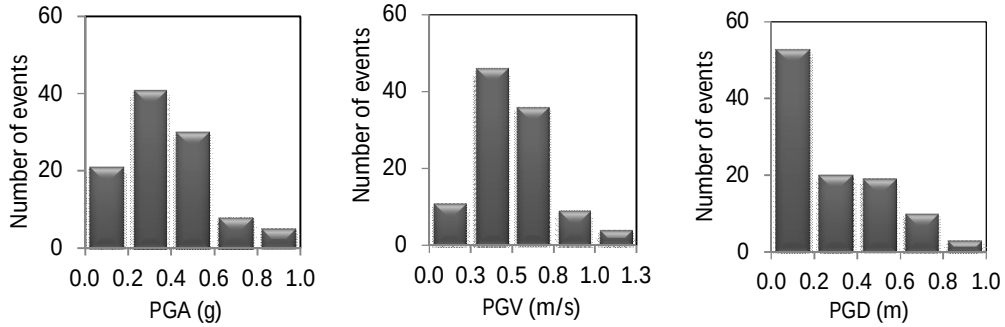

Fig. 4. Distribution of PGA, PGV and PGD of selected ground motions

5. CREST SETTLEMENT OF EMBANKMENT DAMS AND GROUND MOTION INTENSITY INDICES

GMIIs proposed by different researchers describe the capacity of various ground motions to damaged structures, as described in Section 2. An intensity index is applicable when it correlates highly with demand response. For example, if the GMII increases or decreases, the response quantity changes accordingly. To observe the applicability of different GMIIs in predicting destructive ground motions on deformable multi-degree systems, the seismic behavior of embankment dams (crest settlement) were studied.

a) Embankment dam characteristics and natural frequencies

Four hypothetical dams with heights of 50 m, 100 m, 150 m, and 200 m and a real embankment dam were studied to consider the effect of dam frequency on dynamic response. The Success dam is a rolled-earthfill embankment 44 m high and 1038 m long. It consists of a central impervious core along with upstream and downstream shells. The shells of the embankment were constructed on in situ recent alluvium that may be susceptible to liquefaction during a seismic event [26]. Two-dimensional plain strain models were used in these nonlinear analyses. Numerical analyses were conducted using FLAC2D based on continuum finite difference discretization using the Langrangian approach. The geometry and mesh pattern of the 50 m high dam (Dam I) and Success dam are illustrated in Fig. 5a and Fig. 5b, respectively. The dimensions of Dams II, III, and IV are 2, 3 and 4 times larger than Dam I, respectively.

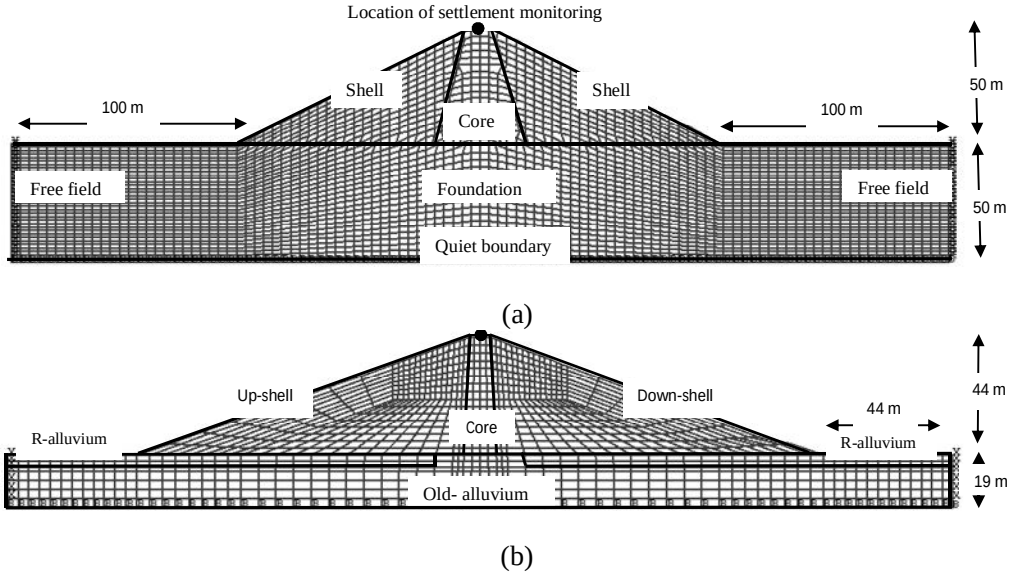

Fig. 5. Geometries, material zones and mesh pattern of: (a) Dam I; (b) Success Dam

As illustrated in Fig. 6, to simulate real boundary conditions, quiet and free-field boundaries available in the code were adapted for the horizontal and lateral boundaries, respectively. For a quiet boundary, dashpots were attached independently to the boundary in the normal and shear directions, providing viscous normal and shear tractions. The quiet boundary prevents the reflection of outward propagating waves back into the model and allows the necessary energy radiation. A free-field boundary enforces free-field motion at the lateral boundaries of the model such that these boundaries simulate the conditions identical to those in an infinite model. In FLAC, the free-field boundaries are coupled with viscous dashpots to simulate a quiet boundary. The foundation and embankment soils of hypothetical dams were modeled as elastic and Mohr-Coulomb elasto-plastic, respectively. In addition, both of these constitutive models were combined with Hardin/Drnevich hysteretic damping to provide energy dissipation in the elastic range [27].

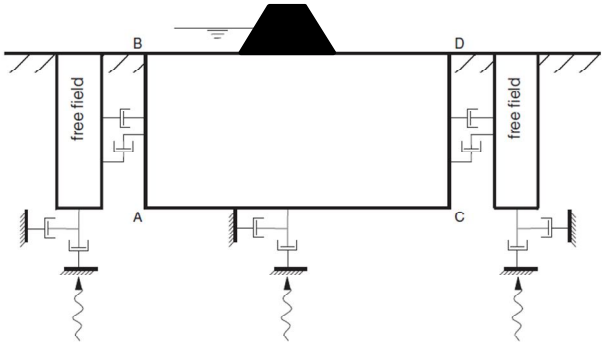

Fig. 6. Boundary conditions of dam models

The dynamic properties of materials used in the analyses of hypothetical dams are presented in Table 3. The modulus reduction factor (G/G_{max}) for different soil types used in embankment dams is shown in Fig. 7a. Fig. 7b shows the profile of shear wave velocity in the dam body. To analyse Success embankment dam, a bounding surface hypoplasticity constitutive model (Wang model) was used. The dynamic properties of materials used in the analyses of Success dam are presented in Table 4 [26]. For an accurate representation of wave transmission through the soil model, the spatial element size (ΔL) must be less than approximately one-tenth the wavelength (λ) associated with the highest frequency component of the input wave. Based upon the elastic properties and mesh size of the FLAC models, the excitation input records were filtered to remove frequencies above 7 Hz before being applied to the models.

The natural frequencies of the dams were calculated to study their effects on the correlation coefficients. To determine the natural frequencies of vibration, the excitation function in Eq. (15) was applied at the crest in the discretized model in the x-direction:

$$f(t) = p_0 \sin(2\pi f_0 t) \quad \text{for } 0 \le t \le t_0 \quad ; \quad f(t) = 0 \quad \text{for } t > t_0 \quad \text{where } t_0 = 1/f_0 \tag{15}$$

Table 3. Dynamic properties of Dam I to Dam IV

	Core	Shell		Foundation
		Upstream	Downstream	
Dry unit weight (kg/m^3)	-	2200	2200	-
Saturated unit weight (kg/m^3)	2200	2350	2350	2400
Poisson's ratio	0.45	0.40	0.40	0.30
Cohesion (N/m^2)	0.0	0.0	0.0	-
Friction angle (degrees)	30.0	45.0	45.0	-

Table 4. Dynamic properties of Success dam

	Core	Shell (US)	Shell (DS)	Recent alluvium (US)	Recent alluvium (DS)	Old alluvium
Void ratio	0.773	0.392	0.39	0.685	0.685	0.620
Friction angle	18–41	37	37	36	36	41
G_0: Model parameter	200	335	336	260	354	1230
κ: Model parameter	0.02	0.002	0.00	0.002	0.002	0.002
h_r: Control stress-	1.663	0.308	0.44	0.189	0.227	1.200
k_r : Control pore pressure generation	100	100	100	1	3	100
d: Control cyclic pore pressure generation	1	1	1	0.55	0.55	1
R_p/ R_f :Dilation line	1	1	1	0.85	0.85	1
b: Control shape of effective stress path	2	2	2	2	2	2

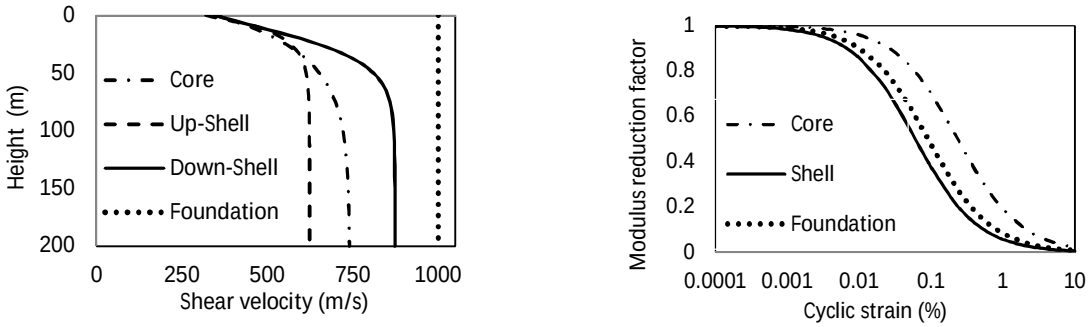

(a) (b)

Fig 7. a) Profile of shear wave velocity in dam body; b) Variation of shear modulus reductions with strain

The problem was analyzed for 25s and the displacement-time history was saved for a select location. At the end of dynamic analysis, a power spectrum analysis was performed on the displacement-time history data set and the results of frequency versus amplitude of the power spectrum were plotted. The frequencies corresponding to the sharp spikes in the amplitude of the power spectrum were read from the frequency-amplitude plot. These frequencies were interpreted to represent the natural frequencies of vibrations of the problem. The lowest frequency value corresponds to the first natural frequency (fundamental frequency). Figure 8 shows the procedures used to determine natural frequencies for a 150 m high dam. The estimated values for the natural frequencies of different dams are presented in Table. 5. It is evident that these are modal frequencies in the elastic range and they constantly change in a nonlinear system as component yielding gradually progresses.

b) Correlation results for embankment dams

Permanent crest settlements were used as nonlinear dynamic response. Figure 9 shows crests settlement time history for Dam II under excitation of record No.17. Values of crest settlement for Dam II under pulse-like ground motions and PGV of these records are summarized in Table. 6. Variations in crest settlement (see Table. 6 for Dam II) versus GMIIs are illustrated in Fig. 10. All correlation coefficients in this study were calculated using Eq. (16). The correlation (ρ) between parameters I and R was measured and the curve with the same form of power function was fitted for *n* parameter pairs and $R = \alpha I^{\beta}$, where α and β are the nonlinear regression parameters. Notice that when the correlation coefficient between I and R was larger, the dispersion was smaller. Also, the correlation coefficient was the same for indices that differ only by a constant or by the exponent (correlation coefficient of a_{sq} equals the correlation coefficient

of the square root of a_{sq} or I_A). For instance, substituting values of Table 6 (assuming PGV=I and crest settlement=R) in Eq. (16), the correlation coefficient between crest settlement and PGV is equal to 0.706. The correlation coefficients between the crest settlement of the embankment dams and GMIIs are summarized in Table 7.

$$\rho = \frac{n\sum(\ln I.\ln R) - \sum \ln I.\sum \ln R}{\sqrt{\left(n\sum(\ln I)^2 - \left(\sum \ln I\right)^2\right)\left(n\sum(\ln R)^2 - \left(\sum \ln R\right)^2\right)}} \quad (16)$$

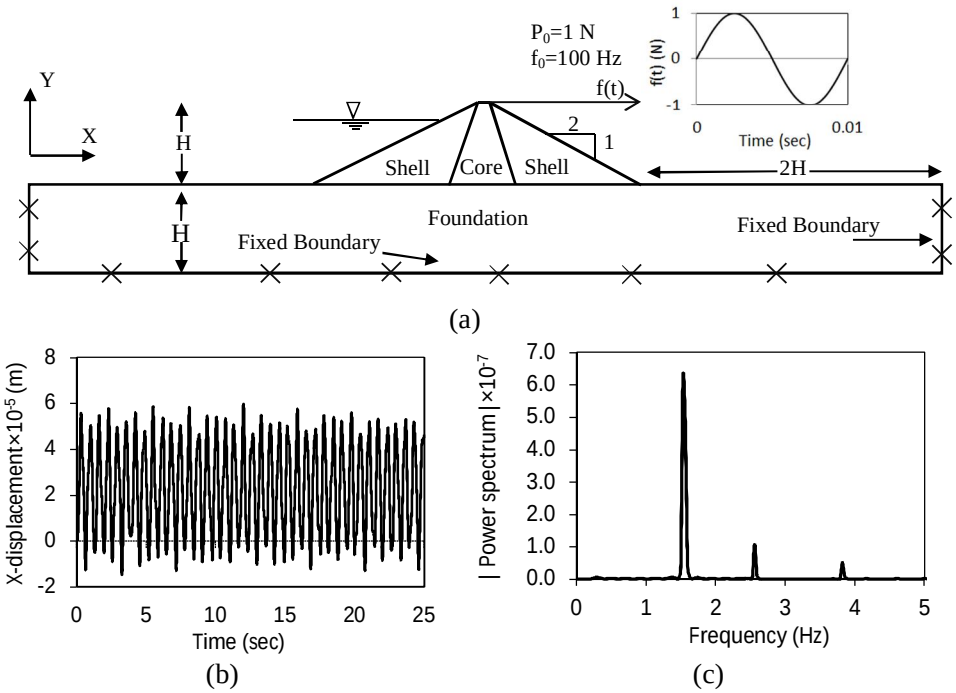

Fig. 8. Natural vibration of Dam III: (a) problem setup for natural frequency determination and applied load; (b) transverse vibrations; (c) natural frequency via FFT power spectrum of (b)

Table 5. Natural frequencies and periods of dams

Model	Height (m)	First natural frequency (Hz)	Natural period (sec)
I	50	2.87	0.35
II	100	1.53	0.65
III	150	1.06	0.94
IV	200	0.81	1.24
Success	44	1.92	0.52

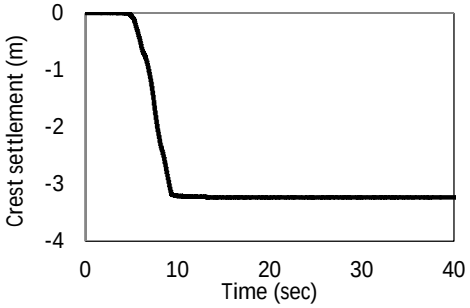

Fig. 9. Crest settlement time history of Dam II under excitation of record No.17

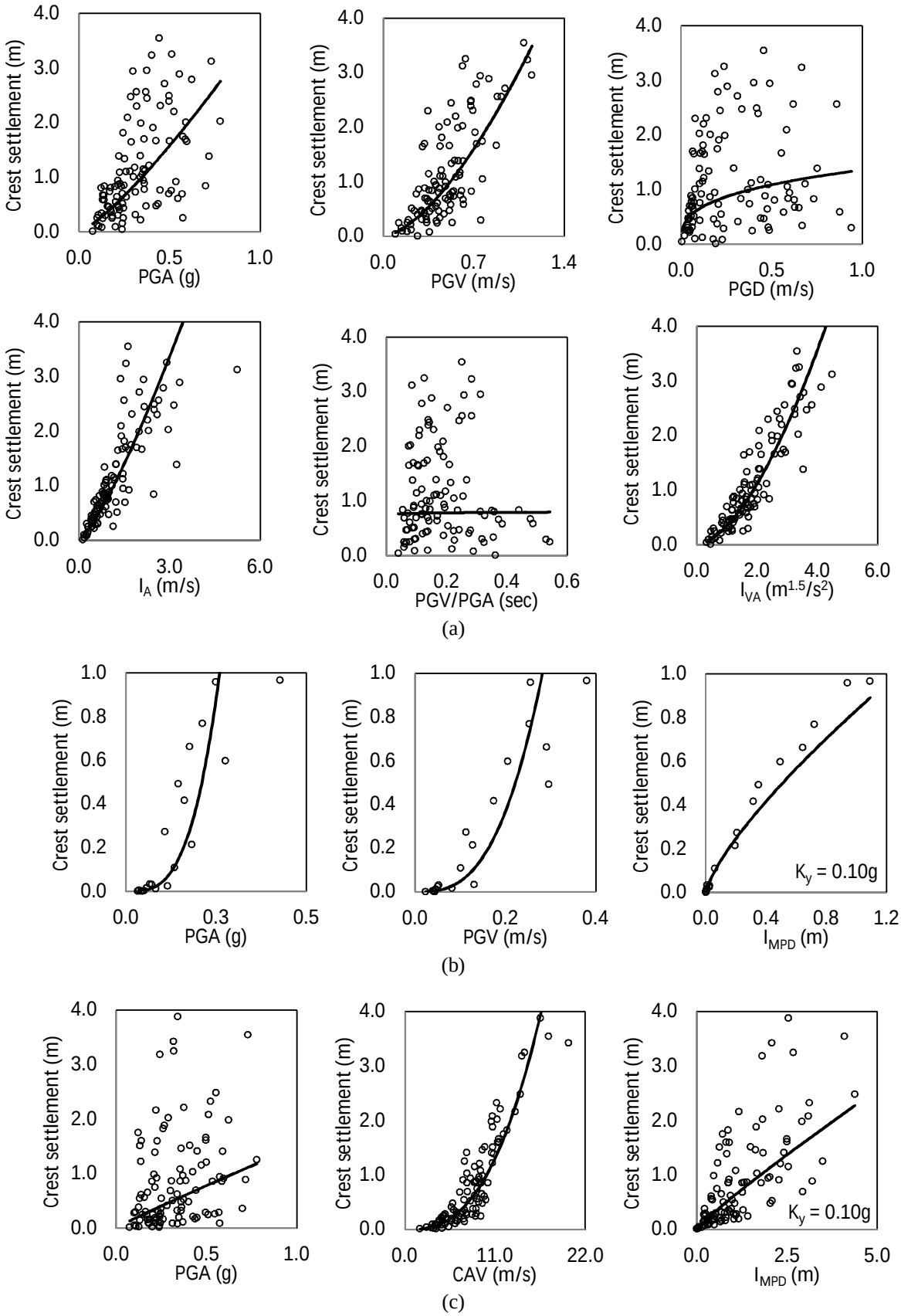

Fig. 10. Relationship between the selected GMIIs and crest settlements for a) Dam II under pulse-like record excitation, b) Dam II under ordinary record excitation; c) Success dam under pulse-like record excitation

Table 6. PGV values of pulse-like records and crest settlement of Dam II

No	PGV (m/s)	S (m)	No	PGV (m/s)	S (m)	No	PGV (m/s)	S (m)	No	PGV (m/s)	S (m)	No	PGV (m/s)	S (m)
1	0.21	0.21	22	0.27	0.00	43	0.20	0.30	64	0.61	3.12	85	0.42	0.24
2	0.64	3.25	23	0.32	0.88	44	0.24	0.47	65	0.32	0.43	86	0.46	1.10
3	0.51	0.76	24	0.41	0.54	45	0.15	0.10	66	0.77	1.74	87	0.41	0.94
4	0.44	1.10	25	0.36	0.45	46	0.52	0.73	67	0.12	0.24	88	0.61	0.83
5	0.53	1.33	26	0.32	1.70	47	0.28	0.86	68	0.88	1.67	89	0.43	0.80
6	0.36	0.08	27	0.38	0.84	48	0.35	2.30	69	0.48	0.69	90	0.35	0.64
7	0.31	1.64	28	0.44	1.65	49	0.30	0.31	70	0.56	2.20	91	0.88	2.56
8	0.09	0.04	29	0.34	0.25	50	0.22	0.51	71	0.72	2.78	92	0.68	2.47
9	0.55	0.73	30	0.30	0.47	51	0.38	0.51	72	0.19	0.09	93	0.58	1.38
10	1.15	2.95	31	0.62	1.38	52	0.45	1.21	73	0.59	1.17	94	0.44	0.34
11	0.47	0.41	32	0.35	0.85	53	0.48	0.91	74	0.51	0.47	95	0.68	0.83
12	0.41	0.94	33	0.39	1.00	54	0.35	1.14	75	0.50	2.09	96	0.62	0.58
13	0.22	0.12	34	0.43	2.01	55	0.55	1.39	76	0.58	1.98	97	0.33	0.30
14	0.41	0.28	35	0.27	0.40	56	0.71	1.91	77	0.45	1.81	98	0.76	0.30
15	0.77	1.05	36	0.26	0.78	57	0.94	2.71	78	0.75	2.94	99	0.53	0.81
16	0.91	2.56	37	0.72	1.69	58	0.82	2.89	79	0.43	0.46	100	0.14	0.15
17	1.12	3.23	38	0.34	0.69	59	0.56	1.08	80	0.53	0.25	101	0.36	0.64
18	1.09	3.54	39	0.61	2.02	60	0.53	2.44	81	0.62	0.67	102	0.42	0.61
19	0.48	1.00	40	0.19	0.25	61	0.51	1.66	82	0.50	0.66	103	0.33	0.37
20	0.59	1.12	41	0.30	0.44	62	0.68	2.49	83	0.52	0.58	104	0.69	2.31
21	0.54	0.83	42	0.32	0.70	63	0.68	2.39	84	0.43	0.88	105	0.60	0.75

It can be concluded from Table 7 that the inelastic structural GMIIs based on decoupling methods were stronger than elastic structural GMIIs for predicting settlement of embankment dams. I_{MPD}, which considers the inelastic behavior of dam for a period of $0.2T_1$ to $1.5T_1$ for each embankment dam was the best index. The correlation coefficient of this GMII with crest settlement was greater than 0.83. In addition, I_{HPD}, which was independent of the dam's natural period, can be used as a good predictor of the crest settlement of embankment dams. As the main difference between near fault and ordinary ground motions lies in velocity time history and not in acceleration, I_{MPD} and I_{HPD} which are a function of acceleration time history, are still suitable GMII for ordinary ground motions. However, efficiency of I_{MPD} compared to old GMIIs is more remarkable for pulse-like ground motions due to greater intensity level which in turn leads to higher nonlinearity behavior.

Elastic structural GMIIs, such as ASI, HI, I_{DC} and $PSa(T_1)$, include the effect of the amplitude of the ground motion over the period selected to cover the possible ranges of response of the structure. The correlation for ASI and I_{DC} were weaker than for HI because the period they covered was much narrower and did not cover the periods of most embankment dams employed here, leading to a higher correlation in the short-to-medium period range. As observed from the results in Table 7, ASI and EPA produced the closest results, mainly because of the similarity of their expressions despite their different definitions. The inadequacy of $PSa(T_1)$ in the nonlinear response region is believed to have been caused by the lack of elongations reflected in the period in the inelastic range.

I_{VA}, which considers the effects of PGV and a_{sq}, was the best predictor of the nonstructural GMIIs. This intensity index reflected the effects of the duration, amplitude and energy of the ground motion but did not consider the properties of the structure. The Arias intensity, PGV and CAV were good predictors of crest settlement and the nonlinear behavior of dams. The displacement related indices GMIIs were the

worst predictors of crest settlement. In addition, PGV/PGA did not show a high correlation with crest settlement.

Table 7. Correlation coefficient (ρ) between crest settlements of embankment dams and ground motion intensity indices (%) for pulse-like records (Pl) and ordinary records (Or)

	Dam-I		Dam-II		Dam-III		Dam-IV		All Dams		Success	
	Pl	Or	Pl	Or	Pl	Or	Pl	Or	Pl-Rank**	Or-Rank	Pl	Rank
PGA	57.7	90.6	62.7	92.1	58.8	92.2	59.5	91.2	16	11	39.0	24
I_A a_{sq}	87.8	95.5	88.5	97.5	85.9	96.7	86.5	96.5	4	3	81.9	4
a_{ms}	56.7	93.7	60.9	93.2	57.3	92.4	57.9	92.4	18	9	37.3	25
I_a	76.2	91.0	79.3	94.2	75.9	94.3	76.7	93.2	9	8	66.1	10
PGV	74.5	85.9	70.6	93.4	70.6	94.0	72.8	92.5	11	12	64.8	11
v_{sq}	56.1	78.9	49.5	88.1	51.1	89.2	53.2	87.5	20	20	62.0	13
v_{ms}	64.7	84.9	60.6	92.4	60.8	93.4	63.5	91.7	15	14	57.3	14
I_F	67.8	83.2	62.2	91.6	63.2	92.1	65.1	90.6	14	17	67.7	9
I_v	57.0	79.6	50.6	88.8	52.3	89.4	53.8	87.9	19	19	64.1	12
CAV	75.0	92.9	71.3	96.5	71.1	95.9	71.0	95.7	12	6	90.2	1
PGD	39.7	63.6	31.5	74.9	33.7	77.1	34.9	75.2	22	22	45.8	18
d_{sq}	29.9	53.9	21.4	65.0	23.7	67.6	24.5	65.9	25	25	41.5	20
d_{ms}	35.1	57.2	26.9	67.9	29.1	70.3	30.2	68.7	23	24	41.0	21
I_d	34.4	58.9	26.1	70.7	28.7	72.8	29.6	71.0	24	23	44.5	19
CAD	43.9	73.7	36.6	83.1	38.8	84.3	40.3	82.8	21	21	56.9	15
PGV/PGA	8.6	15.6	0.9	28.8	4.4	29.9	5.5	28.5	26	26	17.2	26
I_{VA}	89.9	93.0	88.7	97.2	87.0	96.9	88.3	96.2	3	4	82.0	3
EPA ASI	59.2	93.5	61.4	90.8	58.2	89.1	58.8	90.3	17	13	39.5	23
EPV	79.4	84.4	84.0	92.0	85.1	92.7	85.5	90.8	7	15	71.1	8
HI	84.6	85.7	84.9	94.1	85.9	94.1	90.0	92.4	6	10	74.2	6
$PSa(T_1)$	65.5	93.4	76.4	94.9	83.2	92.7	85.4	93.9	8	7	47.5	16
I_{DS}	60.0	93.8	77.2	96.2	81.9	96.2	87.8	95.7	10	5	40.8	22
ND*	69.1	94.6	71.0	88.3	69.7	86.6	71.7	88.6	13	16	46.2	17
$PDD(T_1)$	89.2	96.5	87.8	82.7	88.6	85.2	82.6	89.4	5	18	73.6	7
I_{MPD}	91.6	98.5	97.3	99.0	97.4	98.7	97.4	98.3	1	1	83.3	2
I_{HPD}	92.7	94.9	93.7	98.9	95.0	99.2	97.2	97.5	2	2	81.8	5

*Inelastic GMIIs were calculated by assuming k_y=0.1g.
**Ranks were calculated based on mean value of correlation coefficients of four hypothetical dams.

Results show that there was no significant difference between the correlation coefficients of the dams in this study. This is probably because these dams were located in short-to-medium period ranges and their natural periods were not significantly different. Moreover, as the nonlinear behavior of the multi-degrees of freedom system increased, frequencies different from the modal frequency participated in the response. Thus, the clear difference seen in SDOF systems was not seen in these dams. It must be noted that, if linear formulation was used to calculate the correlation coefficients, the newly proposed correlation confections still show a higher correlation with crest settlement compared to older ones.

Finally, note that GMIIs were not applied to predict the exact value of response, but to predict the trend of demand response (increase or decrease) based on the value of GMII. Thus, to calculate I_{MPD} and I_{HPD}, a rough estimation of the value of yield acceleration is usually sufficient, although an exact value is preferred. However, in estimating ky, using a value less than the exact value of ky leads to more reliable results compared to a value which is greater; Fig. 11 is an example of the variation of crest settlement

against I_{MPD} at three values of yield acceleration. As seen, the correlation coefficients did not change significantly by changing k_y = 0.05 g to k_y = 0.15 g.

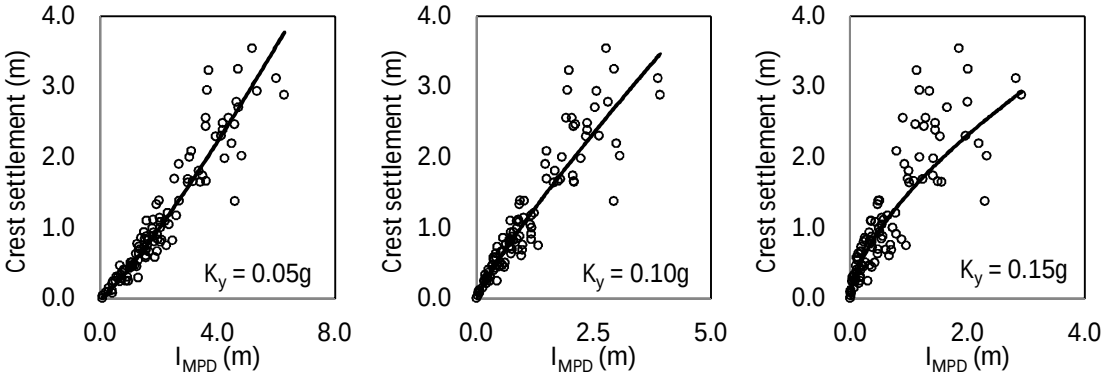

Fig. 11. Variation of crest settlement for Dam II versus I_{MPD} at three yield acceleration: a) k_y = 0.05 g; b) k_y = 0.1 g; b) k_y = 0.15 g

6. CONCLUSION

Based on a comprehensive nonlinear analysis of embankment dams, the correlations between the intensity indices of near-fault ground motions and major seismic responses of geotechnical structures, three new ground motion intensities were proposed in this study. A database of 105 unscaled pulse-like and 20 ordinary earthquake ground motion records was selected. The crest settlements of five embankment dams of different heights were investigated by carrying out 680 non-linear time history analyses and correlating them with ground motion intensity indices. The following conclusions can be drawn from this study:

1. In general, I_{VA} is the best intensity index to correlate with crest settlement for nonstructural ground motion intensity. It is the square root of the product of peak ground velocity and plain integral of the squared acceleration. In addition, CAV illustrates high correlation with crest settlement for Success dam which is constructed on liquefiable material.
2. The Housner intensity covers a wider range of periods for embankment dams than other elastic structural GMIIs and has a higher correlation with the seismic response of the dams.
3. I_{MPD}, which calculates the mean permanent displacement of an SDOF system based the decoupled method over a period of $0.2T_1$ to $1.5T_1$ for an embankment dam, is the best index to correlate with the crest settlement of embankment dams.

The present study was limited to embankment dams which were modeled with plain strain condition. More studies with 3D models, different geometries and dynamic properties are needed to gain a more complete understanding about ranking of different GMIIs.

Acknowledgements: This paper is a part of a research project entitled “Effect of Near Field Ground Motion on Seismic Behavior of Embankment Dams” funded by the International Institute of Earthquake Engineering and Seismology (IIEES) under activity code 6129 and project code 461. This support is gratefully acknowledged.

NOMENCLATURE

PGA	peak ground acceleration	I_A	Arias intensity
a_{sq}	square acceleration	I_a	Riddell acceleration intensity
a_{ms}	mean square acceleration	PGV	peak ground velocity
v_{sq}	square velocity	v_{ms}	mean square velocity
I_F	Fajfar intensity	Iv	Riddell velocity intensity

CAV	cumulative absolute velocity	PGD	peak ground displacement
d_{sq}	square displacement	d_{ms}	mean square displacement
I_d	Riddell displacement intensity	CAD	cumulative absolute displacement
I_{VA}	square root of product of peak ground velocity and square acceleration	EPA	effective peak acceleration
ASI	acceleration spectrum intensity	EPV	effective peak velocity
HI	Housner Intensity	PSa(T1)	pseudo spectrum acceleration at natural period (T_1)
I_{DS}	mean of elastic response spectrum of SDOF system over a period of $0.2T_1$ to $1.5T_1$	ND	Newmark displacement
PDD (T_1)	permanent displacement of SDOF System at Natural period	I_{MPD}	mean permanent displacement of SDOF system over a period of $0.2T_1$ to $1.5T_1$
I_{HPD}	mean permanent displacement of SDOF system over a period of 0.1 to 2.5 sec		

REFERENCES

1. Somerville, P. G. (2003). Magnitude scaling of the near-fault rupture directivity pulse. *Physics Earth Planetary Inter.*, Vol. 137, No. 1, pp. 201-212.
2. Akkar, S. & Ozen, O. (2005). Effect of peak ground velocity on deformation demands for SDOF systems. *Earthq. Eng. Struc. Dyn.*, Vol. 34, pp. 1551-1571.
3. Riddell, R. (2007). On ground motion intensity indices. *Earthquake Spectra*, Vol. 23, No. 1, pp. 147-173.
4. Akkar, S., Yazgan, U. & Gulkan, P. (2007). Drift estimates in frame building subjected to near-fault motions. *J. Struct. Eng.*, Vol. 131, 7, pp. 1014-1024.
5. Elenas, A. (2000). Correlation between seismic acceleration parameters and overall structural damage indices of buildings. *Soil Dyn. Earthq. Eng.*, Vol. 20, pp. 93-100.
6. Elenas, A. & Meskouris, K. (2001). Correlation study between seismic acceleration parameters and damage indices of structure. *Eng. Struct.*, Vol. 23, pp. 698-704.
7. Saygili, G. & Rathje, E. M. (2008). Empirical predictive models for earthquake-induced sliding displacements of slopes. *J. Geotech. Geoenviron. Eng,*, Vol. 134, No. 6, pp. 790-803.
8. Yang, D., Pan, J. & Li, G. (2009). Non-structure-specific intensity measure parameters a characteristic period of near-fault ground motions. *Earthq. Eng. Struc. Dyn.*, Vol. 38, 11, pp. 1257-1280.
9. Bayraktar, A. (2009). Comparison of near- and far-fault ground motion effects on the nonlinear response of dam-reservoir-foundation systems. *Nonlin. Dyn.*, Vol. 58, pp. 655-673.
10. Gazetas, G., Garini, E., Anastasopoulos, I. & Georgarakos, T. (2009). Effects of near-fault ground shaking on sliding systems. *J. Geotech. Geoenviron. Eng*., Vol. 135, No. 12, pp. 1906-1921.
11. Bray, J. D. & Travasarou, T. (2007). Simplified procedure for estimating earthquake-induced deviatoric slope displacements. *J. Geotech. Geoenviron. Eng*., Vol. 133, No. 4, pp. 381–392.
12. Arias, A. (1970). A measure of earthquake intensity in: S*eismic Design for Nuclear Power Plants*, Hansen, R.J. (Ed.), MIT Press, Cambridge, MA, pp. 438-483.
13. Fajfar, P., Vidic, T. & Fischinger, M. (1990). A measure of earthquake motion capacity to damage medium-period structures. *Soil Dyn. Earthq. Eng.*, Vol. 9, No. 5, pp. 236–242.
14. Riddell, R. & Garcia, J. E. (2001). Hysteretic energy spectrum and damage control. *Earthq. Eng. Struc. Dyn.*, Vol. 30, No. 12, pp. 1791–1816.
15. Housner, G. W. (1952). *Intensity of ground motion during strong earthquake*, California Institute of Technology, Pasadena, CA.
16. Von Thun, J. L., Roehm, L. H., Scott, G. A. & Wilson, J. A. (1988). Earthquake ground motions for design and analysis of dams in: *Recent Advances in Ground Motion Evaluation, Geotechnical Special Publication 20, ASCE*, New York, pp. 463-81.

17. Applied Technology Council. (1978). *Tentative Provisions for the Development of Seismic Regulations for Buildings*, ATC 3-06, ATC, Redwood City, CA.
18. ASCE. (2006). Minimum design loads for buildings and other structures, ASCE Standard No. 007–05, *American Society of Civil Engineers*.
19. FEMA. (2001). NEHRP recommended provisions for seismic regulations for new buildings and other structures, 2000 Edn., *Part 1: Provisions. FEMA 368, Building Seismic Safety Council for the Federal Emergency Management Agency, Washington DC.*
20. Newmark, N. M. (1965). Effects of earthquakes on dams and embankments. *Géotechnique*. Vol. 15, No. 2, pp. 139-160.
21. Watson-Lamprey, J., Abrahamson, N. A. (2006). Selection of ground motion time series and limits on scaling. *Soil Dyn. Earthq. Eng.*, Vol. 26, No. 5, pp. 477-482.
22. Wu, J. H. & Chen, C. H. (2009). Back calculating the seismic shear strengths of the tsaoling landslide associated with accelerograph and GPS data. *Iranian Journal of Science & Technology, Transaction B: Engineering*, Vol. 33, No. B4, pp. 301-311.
23. Lin, J. S. & Whitman, R. V. (1983). Decoupling approximation to the evaluation of earthquake-induced plastic slip in earth dams. *Earthq. Eng. Struc. Dyn.*, Vol. 11, pp. 667–678.
24. Chopra, A. K. & Zhang, L. (1991). Earthquake-induced base sliding of concrete gravity dams. *Struct. Eng.*, Vol. 117, No. 12, pp. 3698–3719.
25. PEER. (2006). *Next Generation Attenuation Database*. Pacific Earthquake Engineering Research Center, http://peer.berkeley.edu/nga/index.html .
26. Wang, Z., Makdisi, F. & Egan, J. (2006). Practical applications of a nonlinear approach to analysis of earthquake-induced liquefaction and deformation of earth structures. *Soil Dyn. Earthq. Eng.*, Vol. 26, No. 2, pp. 231-252.
27. Itasca Consulting Group Inc., FLAC User Guide, 3rd Edn., FLAC Version 5.0 (2005).